Evaluation of the bond performance in FRP-brick components re-bonded after initial delamination

Bahman Ghiassi[1], Jose Xavier[2], Daniel V. Oliveira[3], Arkadiusz Kwiecien [4], Paulo B. Lourenço[5], Boguslaw Zajac[6]

ABSTRACT

The bond behavior between Fiber Reinforced Polymers (FRPs) and masonry substrates has been the subject of many studies during the last years. Recent accelerated aging tests have shown that bond degradation and FRP delamination are likely to occur in FRP-strengthened masonry components under hygrothermal conditions. While an investigation on the possible methods to improve the durability of these systems is necessary, the applicability of different bond repair methods should also be studied.

This paper aims at investigating the debonding mechanisms after repairing delaminated FRP-strengthened masonry components. FRP-strengthened brick specimens, after being delaminated, are repaired with two different adhesives: a conventional epoxy resin and a highly flexible polymer. The latter is used as an innovative adhesive in structural applications. The bond behavior in the repaired specimens is investigated by performing single-lap shear bond tests. Digital image correlation (DIC) is used for deeper investigation of the surface deformation and

[1]Postdoctoral Researcher, ISISE, University of Minho, Department of Civil Engineering, Azurém, 4800-058 Guimarães, Portugal. Phone: +351 253 510 499, fax: +351 253 510 217, E-mail: bahmanghiassi@civil.uminho.pt
[2]Research assistant, University of Trás-os-Montes and Alto Douro, UTAD, CITB, Quinta de Prados, 5000-801 Vila Real, Portugal, jmcx@utad.pt.
LOME/INEGI, Rua Dr. Roberto Frias, 4200-465 Porto, Portugal.
[3]Associate Professor, ISISE, University of Minho, Department of Civil Engineering, Azurém, 4800-058 Guimarães, Portugal. Phone: +351 253 510 247, fax: +351 253 510 217, E-mail: danvco@civil.uminho.pt
[4] Associate Professor, Cracow University of Technology, Faculty of Civil Engineering, Cracow, Poland, E-mail: akwiecie@pk.edu.pl
[5] Professor, ISISE, University of Minho, Department of Civil Engineering, Azurém, 4800-058 Guimarães, Portugal. Phone: +351 253 510 209, fax: +351 253 510 217, E-mail: pbl@civil.uminho.pt
[6] Assistant Professor, Cracow University of Technology, Faculty of Civil Engineering, Cracow, Poland, E-mail: bz@limba.wil.pk.edu.pl

strains development. The effectiveness of the repair methods is discussed and compared with the strengthened specimens.

Keywords: *Repair; Bond; FRP; Masonry; Digital image correlation; Delamination.*

1 Introduction

Most masonry structures and historical heritage are vulnerable to the course of time and accidental actions and require structural improvements, using traditional techniques or innovative solutions. Several strengthening and intervention techniques have thus been proposed and used by researchers and professionals during the last years. The focus has been mostly on improvement of the in-plane and out-of-plane resistance of masonry components, while issues such as long-term performance, durability and sustainability have only recently received attention.

Externally bonded reinforcement (EBR) of masonry components with composite materials such as Fiber Reinforced Polymers (FRPs) has been accepted as an effective strengthening solution. Experimental studies have been carried out on the effectiveness of this strengthening technique, see e.g. [1–4], while few numerical models have been developed for simulating the complex nonlinear behavior of FRP-strengthened masonry elements, see e.g. [5,6].

It is well known that the effectiveness of EBR strengthening is intrinsically dependent on the bond performance between the composite material and the masonry substrate [7]. Several researchers have focused during the last years on experimental, numerical and analytical modeling of the bond behavior in FRP-strengthened masonry, see e.g. [7–16]. The experimental tests have been conducted on different substrates (including stone, brick or masonry prism) strengthened with various FRP composites. Valluzzi et al. [12] presented the results of 280 bond tests of masonry bricks strengthened with different composite materials (CFRP, BFRP, GFRP and SRG). Different test setups (single-lap and double-lap) were used for performing the tests in different laboratories. The results show that the failure generally occurred by detachment of a thin layer of the brick, although detachment of a thick irregular layer of the brick has also been

reported by other researchers, see e.g. [17]. A small difference was reported in [12] between the experimental results obtained from the single-lap and double-lap shear tests. Based on the experimental results, several bond-slip laws are adopted and proposed by researchers numerical modeling purposes, see e.g. [9,13].

Recent experimental accelerated ageing tests have shown that bond degradation and FRP delamination may occur in FRP bonded masonry components due to moisture attack or thermal incompatibility between masonry bricks and FRP composites [18,19]. FRP delamination may also occur due to poor workmanship or substrate surface preparation. While it is necessary to investigate the methods to improve the durability of these systems, the possibility of repairing (re-application of) the FRP delaminations and the effectiveness of different repair methods have also to be investigated which are the main subjects of this study. It should be noted that the strips delamination frequently leads to a considerable removal of the material composing the support (which does not remain adherent to the strip). In these cases, filling the removed area with a new material can be a suitable solution. The latter is out of the scope of this study and should be further investigated.

This paper aims at investigating the debonding mechanism in FRP-brick specimens at the initial state (after strengthening) and after repair (re-application of the FRP composite to the bricks' surface after delamination tests). The specimens are strengthened and repaired with two different adhesives: a conventional epoxy resin and a highly flexible polymer (called PS polymer hereafter). The effectiveness of each adhesive on the bond performance at both states is investigated with the aim of Digital Image Correlation technique (DIC). The PS polymer is used as an innovative adhesive for structural strengthening solutions. The use of this polymer for re-application of FRP sheets to the bricks' surfaces after delamination tests has been recently

reported in [20,21] and this paper is considered as a continuation of the experimental tests started by the authors.

Digital Image Correlation (DIC) technique is used for full-field measurement of deformation and strains development by comparing the similarity between image features recorded at different mechanical states. This method has been widely used for measurement of displacements in different fields of solid mechanics, see e.g. [22–27]. However, use of this technique for investigating the interfacial bond behavior has only recently received attention, see e.g. [28–32]. This technique has been successfully used in better understanding the strain and stress transfer mechanisms, the evaluation of the effective bond length and in the extraction of the bond-slip laws.

2 Experimental program and specimens

The aim of this study is to investigate the effectiveness of repairing (re-application of) the FRP-strengthened masonry components after delamination. The experimental program includes performing single-lap shear bond tests on GFRP-strengthened bricks followed by re-application of the delaminated FRP sheets and performing the bond tests on the repaired specimens, see **Fig.1**. The full program includes preparation and testing of 25 specimens in total. The DIC technique is used during the debonding tests for full-field monitoring of the strain development on the specimens' surfaces.

The specimens consist of solid clay bricks with dimensions of 200×100×50 mm^3 as the substrate and a commercial unidirectional glass fiber (MapeWrap G UNI-AX) as the repair/strengthening material bonded to the bricks' surfaces following the wet lay-up procedure. Two different adhesives are used for impregnation and bonding the FRP sheets to the substrate to investigate

the effect of adhesive properties on the effectiveness of the strengthening/repair. The first adhesive is a commercial epoxy resin (MapeWrap 31) previously used by the authors in [30] for preparation of FRP-strengthened brick specimens, which has average tensile strength and elastic modulus of 53.8 MPa and 2.52 GPa, respectively. The second adhesive is a highly flexible polyurethane polymer, called PS hereafter, with average tensile strength and elastic modulus (provided by the manufacturer) of 2.2 MPa and 8.0 MPa, respectively [33].

Mechanical tests are performed on the materials following the applicable test standards and the results are presented in **Table 1**, where CoV indicates the coefficient of variation. The compressive strength of the brick is obtained by performing compressive tests on 40 mm high brick cubes, in the flatwise direction with a 50 kN Lloyd testing machine according to EN 772-1 [34]. Tensile strength and elastic modulus of the epoxy resin and GFRP coupon are determined from tensile tests performed according to ISO 527-1 [35]. The tests are carried out with an Instron testing machine at the displacement rate of 0.01 mm/min. The real mechanical properties of the PS polymer (average tensile strength and elastic modulus of 2.87 MPa and 14.8 MPa, respectively) are taken from previous experimental results, obtained from tensile tests performed according to ISO 527-1 [35], carried out with a Zwick testing machine at the strain rate of 100 %/min.

The prepared specimens can be categorized into four groups as illustrated in **Fig.1**, where **S** indicates a reference Strengthened specimen, **R** indicates a Repaired strengthened specimen, **E** indicates Epoxy and **F** indicates the Flexible polymer:

- SE-specimens (SEa and SEb): bricks strengthened with GFRP using the conventional epoxy resin;
- RE-specimens: delaminated SE-specimens repaired with the conventional epoxy resin;

- SF-specimens: bricks strengthened with GFRP using the PS polymer;
- RF-specimens: delaminated SE-specimens repaired with the PS Polymer.

For preparation of the strengthened SE- and SF-specimens, the GFRP sheets are bonded to the bricks surfaces with the adhesive following the wet lay-up procedure. The bricks are initially washed and dried in the oven for about 24 hours at 100°C. After cooling down, a primer layer is applied to the original surface of the bricks (without application of any physical surface treatment such as grinding or sandblasting) for preparation of the substrate. Finally, the adhesive is used for the matrix for the fibers impregnation and for adhesion to the masonry substrate. The procedure followed for preparation of the strengthened specimens is illustrated in **Fig.2** and **Fig.3**. All the specimens have the same geometrical details consisting of 50 mm FRP widths applied along a length of 150 mm on the brick with a 40 mm unbonded part at the loaded end, see **Fig.4**.

For preparation of the repaired RE- and RF-specimens, the ten SE-specimens are debonded under single-lap shear bond tests after curing in the laboratory conditions, see **Sec. 3** for the test setup and procedure. The failure mode of the SE-specimens was delamination of a thin layer of the brick (six specimens) or delamination of a brick bulb at the free end (four specimens) of the specimens as shown in **Fig.5**. As it can be observed in the figure, the specimens are divided into two groups (to be repaired with PS polymer and epoxy resin) containing specimens with similar fractured surface conditions. The bricks surfaces are carefully cleaned with air compressor followed by application of a primer layer on the bricks' surfaces. The delaminated GFRP sheets are then bonded again to the bricks' surfaces with the conventional epoxy resin (for the RE-specimens) and with the PS Polymer (for the RF-specimens).

Five specimens are prepared for each group resulting in a total of 25 specimens. The test setup and procedure for the delamination tests are the same for all the specimens and are explained in the next section.

3 Debonding test setup and method

The test setup for performing the single-lap shear bond tests and DIC measurements was previously used by the authors to characterize the bond behavior in GFRP-strengthened brick specimens [30].

A testing apparatus with maximum load capacity of 50 kN is used for conducting the single-lap shear bond tests. A rigid supporting frame is used to support the specimens appropriately and avoid misalignments in the load application, see **Fig.6**. The specimens were pulled monotonically with the displacement rate of 0.3 mm/min. The tests were driven under displacement control using a LVDT placed at the loaded end of the FRP composite. The resulting load was measured by means of a load cell. The surface deformation and strains were determined with the DIC technique.

For application of the DIC technique, a speckle pattern, produced by applying a thin coating of white matt followed by a spread distribution of black dots using spray paint, is applied to the specimens surfaces in the region of interest (ROI). Detailed information on this procedure can be found in [30]. The ARAMIS DIC-2D software by GOM [36,37] was used here. The measurement system was equipped with an 8-bit Baumer Optronic FWX20 camera coupled with a Nikon AF Micro-Nikkor 200mm *f*/4D IF-EDlens (**Table 2**).

In the test set-up, the optical system was positioned facing the surface of the specimen. A laser pointer was used to guarantee the correct alignment of the camera with regards to the specimen.

The working distance (defined between the target surface and the support of the cameras) was set about 1.8 m, leading to a conversion factor of 0.037 mm.pixel^{-1}, see **Table 2**. The aperture of the lens was completely open (minimum depth of field) in order to focus the image on the specimen's surface. The lens aperture was then closed to *f*/11 in order to improve the depth of field during testing. The shutter time was set to 5 ms. The light source was finally adjusted in order to guarantee an even illumination of the target surface and to avoid over-exposition.

Regarding the size of the ROI, the optical system (magnification) and the quality of the granulate (average speckle size) obtained by the spray paint, a facet size of 15×15 pixels^2 was chosen in this study. The facet step was also set to 15×15 pixels^2 in order to avoid statistically correlated measurements. The in-plane displacements were then numerically differentiated in order to determine the strains field. The typical measurements resolution was in the range of 10^{-2} mm and 0.02-0.04 % for displacement and strain evaluation, respectively.

4 Bond test results

The envelopes of the experimental force-slip curves are presented in **Fig.7**. A large increment of debonding force can be observed in the repaired specimens in comparison to the original strengthened specimens. The initial stiffness of the specimens (initial slope of the force-slip curves) is also larger in the repaired specimens. The better bond performance observed in the repaired specimens can be due to a better mechanical interlocking, which is the result of the increased roughness of the bricks surfaces after initial debonding. The debonding slip is similar in SE- and RE-specimens (around 1.2 mm), however an increase is observed from 0.5 mm in SF-specimens to 1.0 mm in RF-specimens.

Table 3 and **Table 4** present the debonding force and failure modes of all the specimens for each group. The average debonding force of the strengthened specimens with the epoxy resin (average of SEa and SEb specimens) is 8.85 kN (CoV=8.3%). Meanwhile, the average debonding force in the specimens strengthened with flexible polymers (SF-specimens) is 5.65 kN (CoV=18.5%) being 33% lower than the SE-specimens. The loss of debonding load observed in the SF-specimens can be attributed to the lower adhesion strength of the PS polymer-to-brick than the epoxy resin-to-brick and the governing failure mode. As can be observed in **Table 3**, all the SF-specimens had an adhesive failure mode at the FRP-brick interface. The weak interface has resulted in the change of failure mode in the composite system and therefore lower debonding strength. Moreover, due to the very low elastic modulus of the PS polymer, the effective bond length can be larger than the actual bonded length (150 mm) resulting in partial development of the bond strength in the tests. This latter issue is further investigated and discussed next with the aim of the DIC measurements.

A large increase is found in the debonding strength of the specimens after repair in comparison to the strengthened specimens. This difference is clearer in the graph presented in **Fig.8**. The average debonding force of the RE-specimens is 16.56 kN (CoV=15.4%), while the debonding force of the corresponding strengthened specimens (SEa-specimens) is 8.48 kN (CoV=8.3%). A large increase in the debonding strength is also observed after repairing the specimens with the PS polymer (RF-specimens). In this case, the average debonding force of the strengthened specimens (SEb-specimens) was 9.23 kN (CoV=6.5%) which increased to 12.92 kN (CoV=13.5%) after repair (RF-specimens). The increments are around 95% and 40% for the RE- and RF-specimens, respectively. The initial delamination tests resulted in removal of the superficial layer of the bricks and therefore increment of surface roughness in the repaired

specimens. Therefore, the interlocking adhesion has increased significantly between FRP and the brick substrate in comparison to the strengthened specimens resulting in higher debonding forces.

The failure mode in the SE-specimens was mostly cohesive with fracture inside a thin layer of the brick or adhesive with formation of a brick bulb at the free end, see **Fig.9**(a). However, the governing failure mode in the SF-specimens was adhesive failure at the polymer-brick interface as shown in **Fig.9**(b). This can be due to the low chemical and mechanical adhesion between the brick surface and the PS polymer in the strengthened specimens.

All the RE-specimens had a cohesive failure with the fracture occurring inside the brick, see **Fig.10**(a). In some cases a brick bulb was also detached at the free end of the specimens. A similar failure mode was also observed in the corresponding strengthened specimens (SEa), see **Table 3**. However, the failure of the RF-specimens changed in comparison to their corresponding strengthened specimens (SEb). The failure mode in these specimens was either cohesive inside the brick or cohesive inside the PS polymer as shown in **Fig.10**(b). This change of failure mode can be due to reduction of stress concentrations caused by many times lower Young's modulus than epoxy resin and strong mechanical interlocking between the PS polymer and the brick surface in the repaired specimens.

5 Strain analysis results

Fig.11 and **Fig.12** present the typical evolution of longitudinal strains on the FRP surface during the debonding tests at different load levels. The full-field strain distributions, determined from the DIC measurements, clearly show the strain transfer zone along the bonded length. It can be observed that longer bonded lengths are contributing to the strain and stress transfer to the

substrate in the RE-specimens in comparison to the SE-specimens, see **Fig.11**. On the other hand, it seems that in SF- and RF-specimens the strains are developed along all the bonded length gradually diminishing near the free end.

The longitudinal strain profiles are extracted from the full-field measurements, by averaging the strains along the FRP width [30], and presented at different load levels for a typical specimen in each group in **Fig.13**. The observed fluctuations in the strain profiles can be partly attributed to the variation of the material properties, bond imperfections and also non-smooth surface of the specimens [30].

In SE and RE-specimens, **Fig.13**(a, b), the strain profiles follow a nonlinear trend reaching zero along the bonded length. Moreover, a sudden increase in the strain level is observed at the final load stages which can be attributed to the initiation of debonding and crack propagation along the bonded length. On the other hand, the strain profiles in SF- and RF-specimens seem to increase linearly until the debonding, **Fig.13**(c, d). Moreover, as it was expected from the higher debonding loads, higher strain levels are developed in the repaired specimens in comparison to strengthened specimens.

The strain distribution in SE- and RE-specimens is approximated with the following nonlinear expression by performing a regression analysis [30]:

$$\varepsilon(x) = A_2 + \frac{A_1 - A_2}{1 + (\frac{x}{x_0})^p} \tag{1}$$

where A_2, A_1, x_0, p are the constants to be determined from experimental results and x is the distance from the loaded end. The predicted strain distribution at the ultimate load level, P_u, is shown with a solid line in **Fig.14**(a, b). It can be seen that the bonded area consists of three main regions as also discussed in [10, 30]. The FRP is fully debonded from the substrate near the

loaded end. This is followed by a stress transfer zone, and afterwards that no stress is transferred to the substrate. The length of the stress transfer zone is called the effective bond length and is around 30 mm and 90 mm for SE- and RE-specimens studied here, respectively (shaded in **Fig.14**(a, b)).

The strain profiles in SF- and RF-specimens increase linearly until the debonding of the FRP from the substrate, **Fig.14**(c, d). A linear expression is thus used for fitting the experimental diagrams. The effective bond length is not distinguishable in the strain profiles showing that, possibly, it is larger than the actual bonded length (150 mm). This, in addition to the low chemical and mechanical adhesion, can be one of the possible reasons for the lower debonding loads observed in these specimens.

Having the strain profiles along the bonded length, it is possible to extract the bond-slip laws defined as the relationship between the local applied shear stress and the FRP slip relative to the brick surface [30]. The FRP slip at distance *x* from the free end of the specimen, assuming a zero slip in the free end, can be obtained by integrating the strain profile along the bonded length as follows:

$$s(x) = \int \varepsilon_f \, dx \tag{2}$$

Subsequently, the shear stress distribution is defined along the bonded length is defined as:

$$\tau(x) = t_f E_f \frac{d\varepsilon_f}{dx} \tag{3}$$

where $d\varepsilon_f / dx$ is the gradient of FRP strain along the sheet length, E_f is the FRP elastic modulus, and t_f is the FRP thickness. The distribution of shear stresses can also help in

estimating the effective bond length can also be defined as the length in which the shear stresses are transferred to the substrate [38]. The typical shear stress distributions obtained with Eq. (3) at the peak load level are presented in **Fig.15**. It should be noted that the fitted curves of the strain profiles, see **Fig.14**, are used here for calculation of the shear stresses. A clear difference of the peak shear stress and the effective bond length can be observed between the SE- and RE-specimens. As the strain profile is linear in case of SF- and RF-specimens due to the short bonded length, the stress profile is constant along the bonded length according to Eq. (3) and therefore the effective bond length is again not distinguishable.

The interfacial bond-slip laws are obtained from the fitted strain profiles according to Eqs. (2, 3) and the results are presented in **Fig.16** and **Fig.17**. A tri-linear bond-slip law is proposed for the SE- and RE-specimens as also used in [30], see **Fig.16**. The bond fracture energy, defined as the area under the bond-slip curve is much larger in the RE-specimens (1.88 N/mm) in comparison to SE-specimens (0.54 N/mm). The maximum bond strength has also increased from 3.4 MPa to 7.5 MPa from SE- to RE-specimens. The increment of mechanical interlocking in the repaired specimens and change of debonding failure mode from fracture inside a thin layer of the brick (in SE-specimens) to a deep fracture inside the brick (in RE-specimens) have resulted in the observed higher fracture energy and maximum bond stresses.

In case of SF- and RF-specimens, the maximum transferrable shear stresses cannot be developed in the composite system due to the short actual bonded length of the specimens, see **Fig.17**. The bond fracture energy in this case is 0.38 N/mm and 0.52 N/mm in SF- and RF-specimens, respectively for the tested specimens. However, for development of the maximum bond stress and fracture energy, preparation of specimens with longer bonded lengths is necessary. This brings in an obvious difficulty in this case, as the brick has a length of 200 mm only.

6 Conclusions

The effectiveness of repairing delamination in FRP-strengthened masonry components was investigated in this study. The specimens consisted of bricks strengthened (denoted by **S**), tested and, subsequently, repaired (denoted by **R**) with GFRP sheets using two different adhesives: a conventional epoxy resin (denoted by **E**) and a highly flexible polyurethane polymer (denoted by **F**) as an innovative strengthening/repair adhesive in structural engineering applications. The effectiveness of strengthening/repair application was studied by performing single-lap shear bond tests. The digital image correlation (DIC) technique was used for investigating the evolution of strains on the specimens' surfaces during the debonding.

For the strengthened specimens, it was observed that the debonding force of the SE-specimens (9.19 kN) was higher than the SF-specimens (5.65 kN). The failure mode in the SE-specimens was mostly cohesive with fracture inside a thin layer of the brick or, in some specimens, with formation of a brick bulb at the free end. However, the governing failure mode in the SF-specimens was adhesive failure at the polymer-brick interface. The lower debonding load observed in the SF-specimens can be due to the lower tensile strength (adhesion) of the PS polymer than epoxy resin, the governing failure mode and the fact that the effective bond length in these specimens was larger than the actual bonded length (150 mm). The latter was concluded from the full-field measurements obtained from the DIC.

As for the repaired specimens, a large increase in the debonding force of the repaired specimens in comparison to the corresponding strengthened specimens was observed. This increase was around 95% for the RE-specimens and 31% for the RF-specimens which is attributed to the improved mechanical interlocking and chemical adhesion in the repaired specimens and

reduction of stress concentrations in the bond interface. The results show the effectiveness of both adhesives in repairing the delaminations in FRP-bonded components.

The strain profiles obtained from the DIC measurements showed that the effective bond length in the SE-specimens was around 30 mm, while this value was around 60 mm for the RE-specimens. The effective bond length in the SF- and RF-specimens was observed to be larger than the actual bonded length. The bond-slip laws of the SE- and RE-specimens were also extracted from the strain profiles. A large increase in the bond fracture energy was observed in the RE-specimens in comparison to SE-specimens. Again, it was not possible to obtain the complete bond-slip laws for the SF- and RF-specimens.

In general, it was observed that repairing the delaminated FRPs with both adhesives improve the bond performance in comparison to the strengthened specimens.

Acknowledgements

The first author acknowledges the financial support of the Portuguese Science Foundation (Fundação de Ciência e Tecnologia, FCT), through grant SFRH/BPD/92614/2013. Additional acknowledgement goes to Sika Poland for providing the PS polymer to the laboratory of the Minho University in Portugal

References

[1] Triantafillou TC. Strengthening of masonry structures using epoxy-bonded FRP laminates. J Compos Constr ASCE 1998;2:96–104.

[2] Gabor A, Bennani A, Jacquelin E, Lebon F. Modeling approaches of the in-plane shear behavior of unreinforced and FRP strengthened masonry panels. Compos Struct 2006;74:277–88.

[3] Marcari G, Manfredi G, Prota A, Pecce M. In-plane shear performance of masonry panels strengthened with FRP. Compos Part B Eng 2007;38:887–901.

[4] Borri A, Castori G, Corradi M. Shear behavior of masonry panels strengthened by high strength steel cords. Constr Build Mater 2011;25:494–503.

[5] Milani G, Milani E, Tralli A. Approximate limit analysis of full scale FRP-reinforced masonry buildings through a 3D homogenized FE package. Compos Struct 2010;92:918–35.

[6] Grande E, Imbimbo M, Sacco E. Finite element analysis of masonry panels strengthened with FRPs. Compos Part B Eng 2013;45:1296–309.

[7] Ghiassi B, Marcari G, Oliveira DV, Lourenço PB. Numerical analysis of bond behavior between masonry bricks and composite materials. Eng Struct 2012;43:210–20.

[8] Panizza M, Garbin E, Valluzzi MR, Modena C. Bond behavior of CFRP and GFRP laminates on brick masonry. Proc. IV Int. Semin. Struct. Anal. Hist. Constr., 2008, p. 763–70.

[9] Grande E, Imbimbo M, Sacco E. Bond behaviour of CFRP laminates glued on clay bricks: Experimental and numerical study. Compos Part B Eng 2011;42:330–40.

[10] Carloni C, Subramaniam K V. FRP-Masonry Debonding : Numerical and experimental study of the role of mortar joints. J Comops Constr ASCE 2012; 16(5):581–9.

[11] Faella C, Camorani G, Martinelli E, Paciello SO, Perri F. Bond behavior of FRP strips glued on masonry: Experimental investigation and empirical formulation. Constr Build Mater 2012;31:353–63.

[12] Valluzzi MR, Oliveira D V, Caratelli A, Castori G, Corradi M, De Felice G, et al. Round robin test for composite-to-brick shear bond characterization. Mater Struct 2012;45:1761–91.

[13] Ghiassi B, Oliveira DV, Lourenço PB, Marcari G. Numerical study of the role of mortar joints in the bond behavior of FRP-strengthened masonry. Compos Part B Eng 2013;46:21–30.

[14] Carrara P, Freddi F. Statistical assessment of a design formula for the debonding resistance of FRP reinforcements externally glued on masonry units. Compos Part B Eng 2014;66:65–82.

[15] Basilio I, Fedele R, Lourenço PB, Milani G. Assessment of curved FRP-reinforced masonry prisms: Experiments and modeling. Constr Build Mater 2014;51:492–505.

[16] Malena M, de Felice G. Debonding of composites on a curved masonry substrate: Experimental results and analytical formulation. Compos Struct 2014;112:194–206.

[17] Carrara P, Ferretti D, Freddi F. Debonding behavior of ancient masonry elements strengthened with CFRP sheets. Compos Part B Eng 2013;45:800–10.

[18] Ghiassi B, Oliveira DV, Lourenço PB. Accelerated hygrothermal ageing of bond in FRP-masonry systems. J Compos Constr 2014, doi: 10.1061/(ASCE)CC.1943-5614.0000506.

[19] Ghiassi B, Oliveira DV, Lourenço PB. Hygrothermal durability of bond in FRP-strengthened maosnry. Mater Struct 2014, doi: 10.1617/s11527-014-0375-7.

[20] Kwiecień A, Zając B. Is it Possible to Repair Detached Composites Effectively after Failure of Masonry Strengthening? Key Eng Mater 2015;624:518–25.

[21] Kwiecień A. Shear bond of composites-to-brick applied with highly deformable, in relation to resin epoxy, interface materials. Mater Struct 2014;47:2005–20.

[22] Grédiac M. The use of full-field measurement methods in composite material characterization: interest and limitations. Compos Part A Appl Sci Manuf 2004;35:751–61.

[23] Dahl KB, Malo KA. Planar Strain Measurements on Wood Specimens. Exp Mech 2008;49:575–86.

[24] Brynk T, Molak RM, Janiszewska M, Pakiela Z. Digital Image Correlation measurements as a tool of composites deformation description. Comput Mater Sci 2012;64:157–61.

[25] Xavier J, Sousa AMR, Morais JJL, Filipe VMJ, Vaz M. Measuring displacement fields by cross-correlation and a differential technique: experimental validation. Opt Eng 2012;51:43602.

[26] Fernandes RMRP, Chousal JAG, de Moura MFSF, Xavier J. Determination of cohesive laws of composite bonded joints under mode II loading. Compos Part B Eng 2013;52:269–74.

[27] Pan B, Yu L, Wu D, Tang L. Systematic errors in two-dimensional digital image correlation due to lens distortion. Opt Lasers Eng 2013;51:140–7.

[28] Fedele R, Scaioni M, Barazzetti L, Rosati G, Biolzi L. Delamination tests on CFRP-reinforced masonry pillars: Optical monitoring and mechanical modeling. Cem Concr Compos 2014;45:243–54.

[29] Gams M, Kwiecień A, Zając B, Tomazevic M. Seismic strengthening of brick masonry walls with flexible polymer coating. 9th Int. Mason. Conf., Guimarães, 2014.

[30] Ghiassi B, Xavier J, Oliveira DV, Lourenço PB. Application of digital image correlation in investigating the bond between FRP and masonry. Compos Struct 2013;106:340–9.

[31] Carloni C, Subramaniam K V. Investigation of sub-critical fatigue crack growth in FRP/concrete cohesive interface using digital image analysis. Compos Part B Eng 2013;51:35–43.

[32] Subramaniam K V., Carloni C, Nobile L. Width effect in the interface fracture during shear debonding of FRP sheets from concrete. Eng Fract Mech 2007;74:578–94.

[33] Kwiecień A. Stiff and flexible adhesives bonding CFRP to masonry substrates investigated in pull-off test and Single-Lap test. Arch Civ Mech Eng 2012;12:228–39.

[34] EN 772-1. Methods of test for masonry units -Part 1: Determination of compressive strength; 2002.

[35] EN ISO 527-1. Plastics-determination of tensile properties- Part 1: general principles; 2012.

[36] Xavier J, de Jesus A, Morais J, Pinto J. Stereovision measurements on evaluating the modulus of elasticity of wood by compression tests parallel to the grain. Constr Build Mater 2012;26:207–15.

[37] ARAMIS user manual- Software- v6.0.2-6. 2009.

[38] Dai J, Ueda T, Sato Y. Unified Analytical Approaches for Determining Shear Bond Characteristics of FRP-Concrete Interfaces through Pullout Tests. J Adv Concr Technol 2006;4:133–45.

List of Tables

List of Figures

Table 1. Material mechanical properties.

Masonry brick			CoV(%)
Compressive strength	f_{cb} (MPa)	14.3	4.0
GFRP coupons			
Tensile strength	f_{tf} (MPa)	1250	15.0
Elastic modulus	E_f (MPa)	79200	6.8
Ultimate deformation	ε (%)	3.0	20.2
Epoxy resin			
Tensile strength	f_{tm} (MPa)	53.8	9.7
Elastic modulus	E_m (MPa)	2500	9.5
Polyurethane polymer (PS)			
Tensile strength	f_{tm} (MPa)	2.9	2.2
Elastic modulus	E_m (MPa)	14.8	12.6

Table 2. Optical system components and measurement parameters.

CCD camera	
Model	Baumer Optronic FWX20 (8 bits, 1624×1236 pixels, 4.4 μm/pixel)
Shutter time	5 ms
Acquisition frequency	1 Hz
Lens	
Model	Nikon AF Micro-Nikkor 200mm *f*/4D
Aperture	*f*/11
Lighting	LEDMHL10 (color temperature: 6000 K)
Working distance	1800 mm
Conversion factor	0.037 mm/pixel
Project parameter – Facet	
Facet size	15×15 pixel^2
Step size	15×15 pixel^2
Project parameter – Strain	
Computation size	7×7 facets
Validity code	55%
Strain computation method	Total
Image recording	
Acquisition frequency	1 Hz

Table 3. Debonding force and failure mode of the SEa, RE and SF specimens.

SEa specimens	P_{max} (kN)	Failure mode*	RE specimens	P_{max} (kN)	Failure mode*	SF specimens	P_{max} (kN)	Failure mode*
SEa1	8.81	CBT	RE1	18.16	CB	SF1	5.27	A
SEa2	7.57	AB	RE2	13.10	CB,CBT	SF2	4.18	A
SEa3	9.43	CBT	RE3	19.39	CBT	SF3	5.94	A
SEa4	8.50	CBT	RE4	14.85	CBT	SF4	5.81	A
SEa5	8.07	CBT	RE5	17.29	CBT	SF5	7.06	A
Average	**8.48**		Average	**16.56**		Average	**5.65**	
Std. Dev.	**0.71**		Std. Dev.	**2.55**		Std. Dev.	**1.05**	
CoV. (%)	**8.3**		CoV. (%)	**15.4**		CoV. (%)	**18.5**	

*A: Adhesive failure at the FRP-brick interface; CA: Cohesive failure inside the adhesive layer; CB: Cohesive failure inside the brick with detachment of a thick layer of the brick; CBT: Cohesive failure inside the brick with detachment of a thin uniform layer of the brick; AB: Debonding with detachment of a brick bulb at the free end.

Table 4. Debonding force and failure mode of the SEb and RF specimens.

SEb specimens	P_{max} (kN)	Failure mode	RF specimens	P_{max} (kN)	Failure mode
SEb1	8.40	AB	RF1	14.93	CA
SEb2	9.51	AB	RF2	10.89	CA
SEb3	9.70	CBT	RF3	13.12	CA
SEb4	8.80	AB	RF4	14.26	CB
SEb5	9.76	CBT	RF5	11.42	CB
Average	**9.23**		Average	**12.92**	
Std. Dev.	**0.6**		Std. Dev.	**1.75**	
CoV. (%)	**6.51**		CoV. (%)	**13.5**	

*A: Adhesive failure at the FRP-brick interface; CA: Cohesive failure inside the adhesive layer; CB: Cohesive failure inside the brick with detachment of a thick layer of the brick; CBT: Cohesive failure inside the brick with detachment of a thin layer of the brick; AB: Debonding with detachment of a brick bulb at the free end.

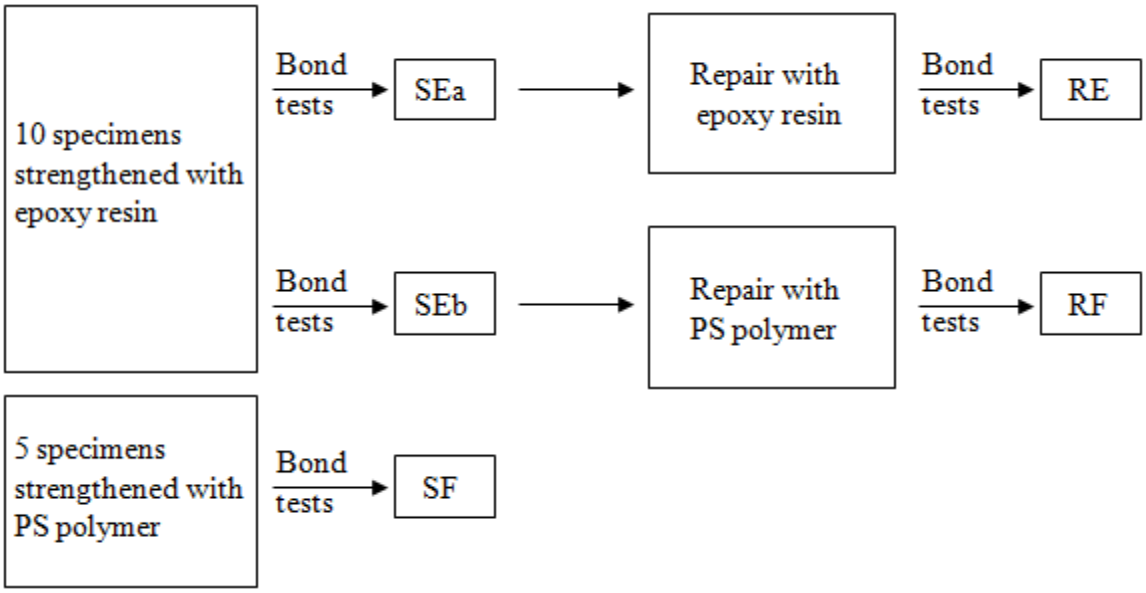

Fig.1. Specimens' preparation and testing program.

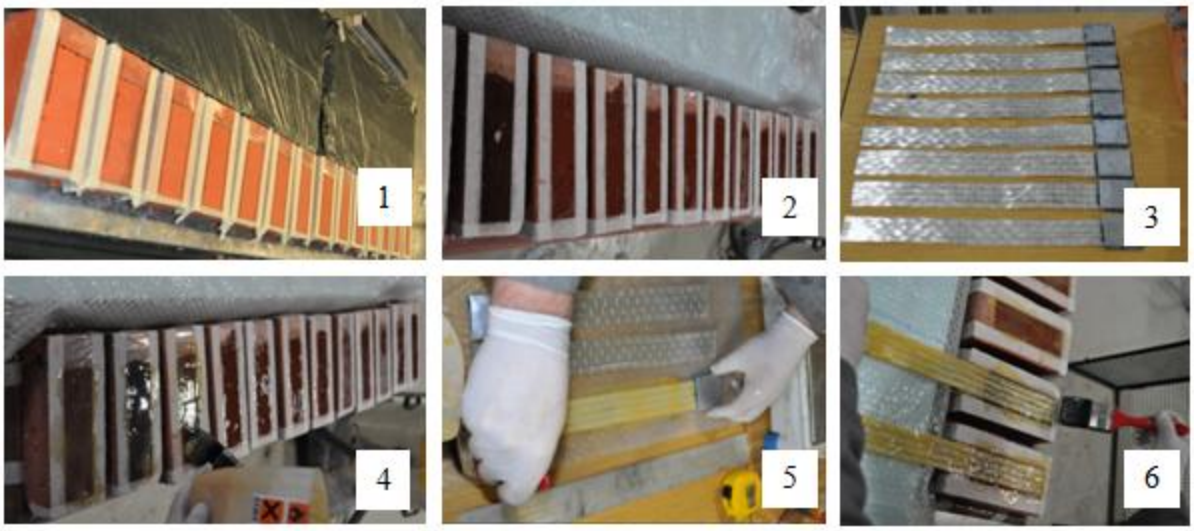

Fig.2. Procedure followed for preparation of the strengthened specimens with epoxy resin (note that the same procedure was followed for specimens prepared with PS polymer).

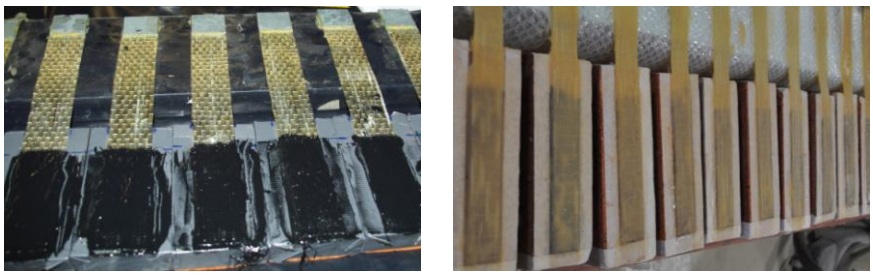

(a) (b)

Fig.3. Strengthened specimens: (a) SE-specimens; (b) SF-specimens.

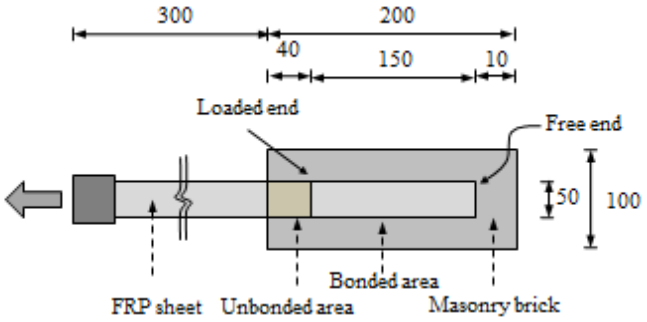

Fig.4. Geometrical details of the specimens (dimensions in mm).

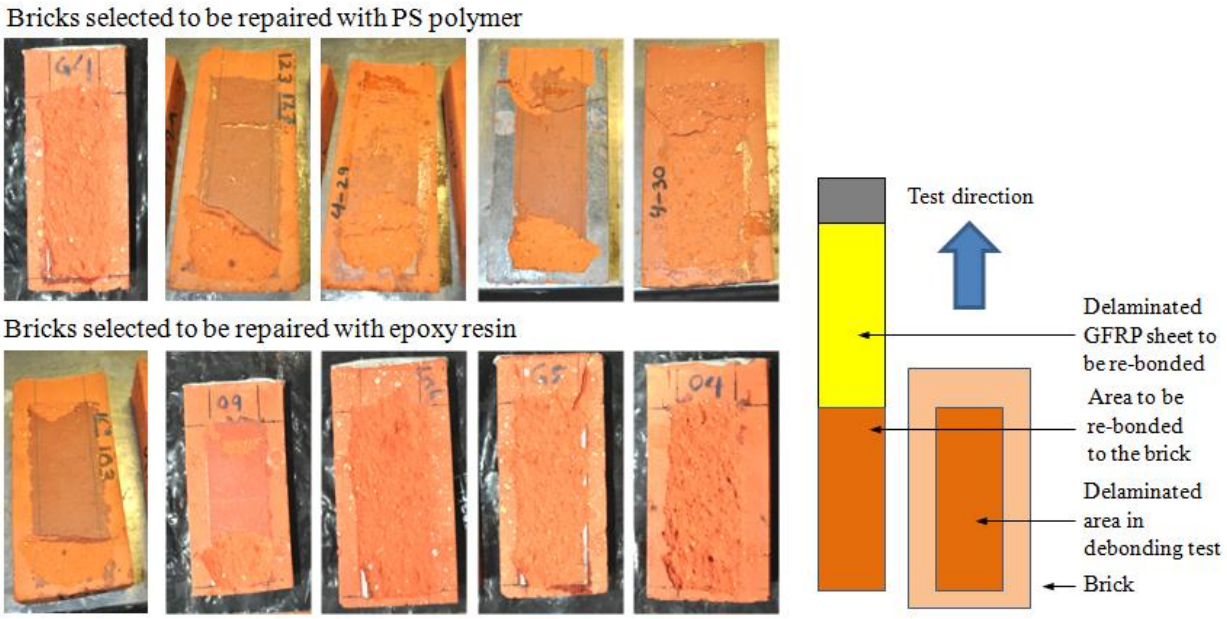

Fig.5. Bricks surfaces after initial delamination tests (used for repair).

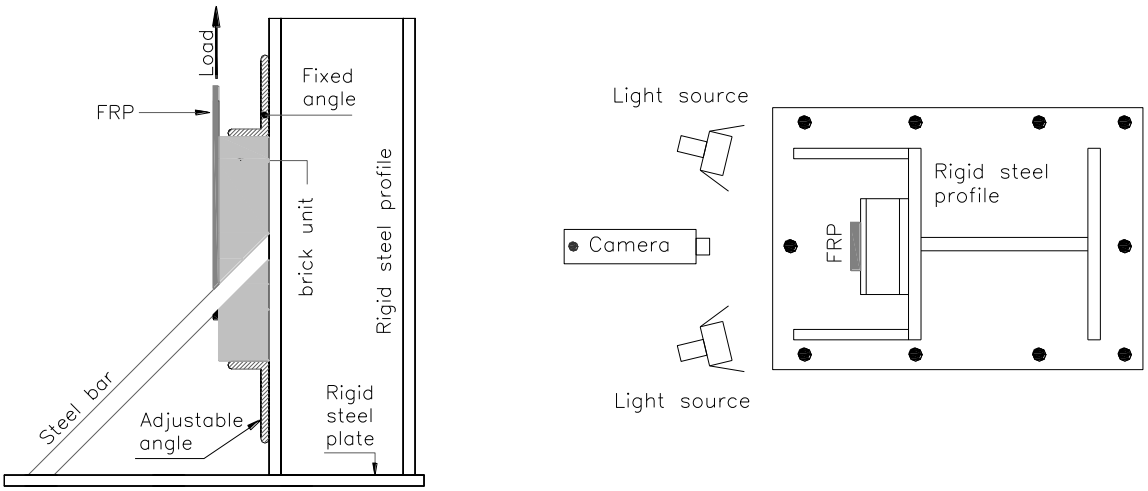

(a) (b)

Fig.6. Shear debonding test setup (a) side view; (b) top view.

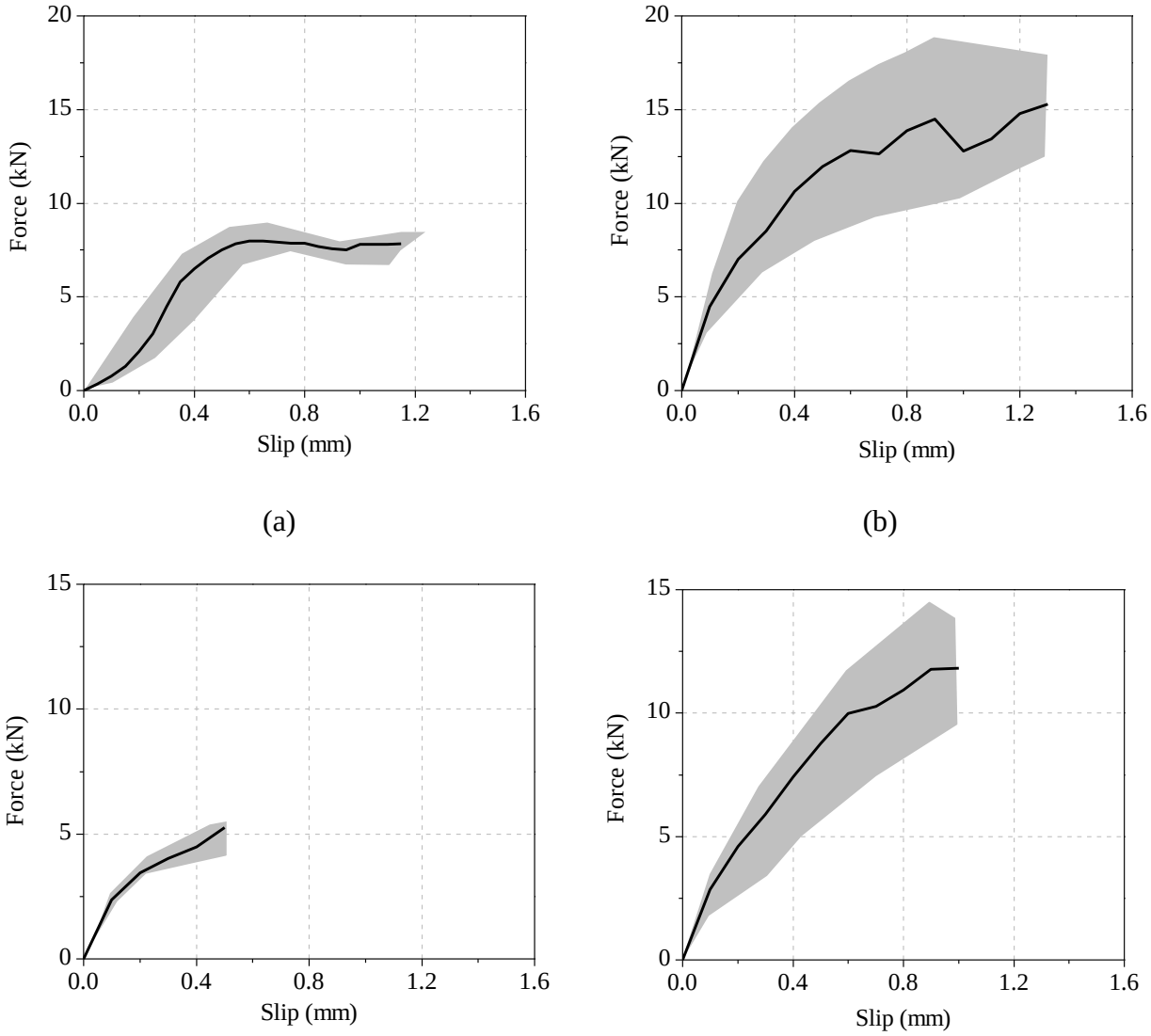

Fig.7. Force-slip curves of: (a) SE-; (b) RE-; (c) SF- and (d) RF-specimens.

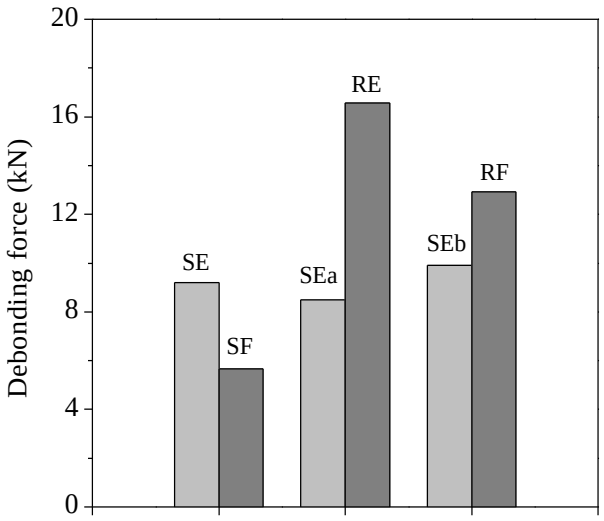

Fig.8. Comparison of average debonding forces.

(a)

(b)

Fig.9. Typical failure modes of (a) SE- and (b) SF-specimens.

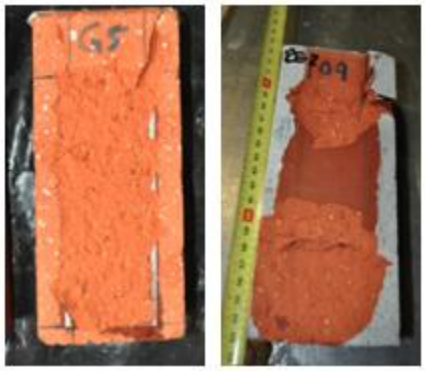

(a)

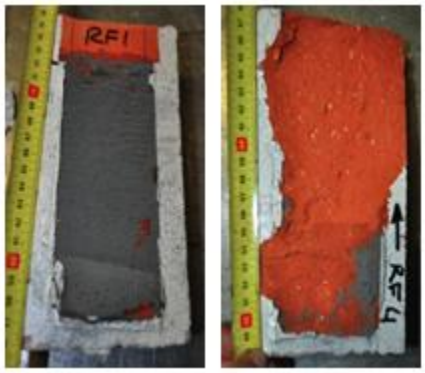

(b)

Fig.10. Typical failure modes of (a) RE- and (b) RF-specimens.

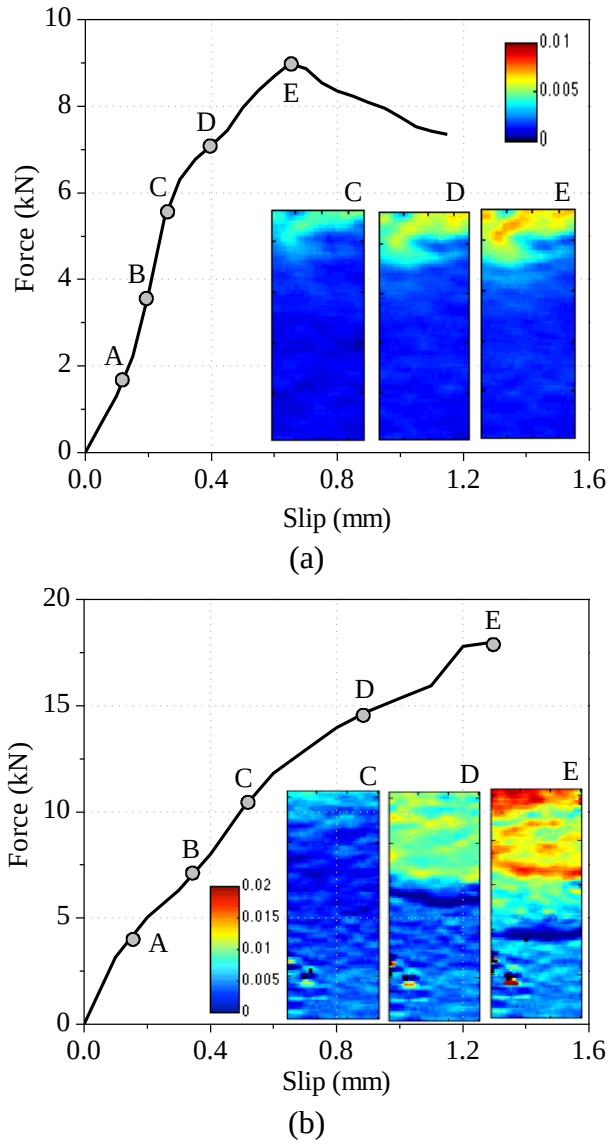

Fig.11. Strain distribution along the bonded area at different load levels in a typical (a) SE- and (b) RE-specimen.

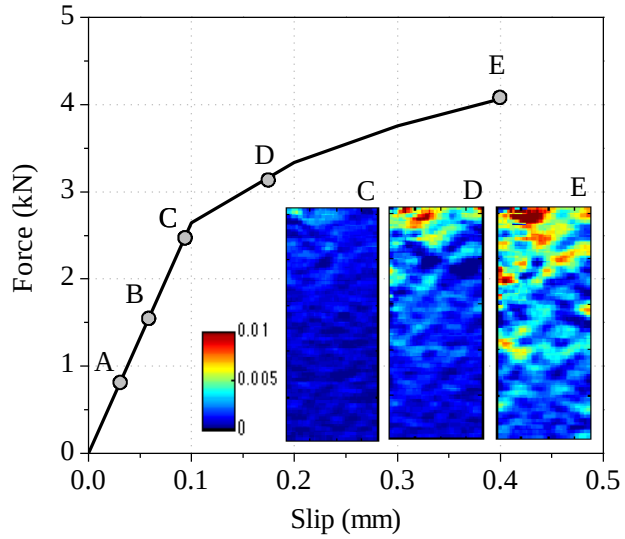

(a)

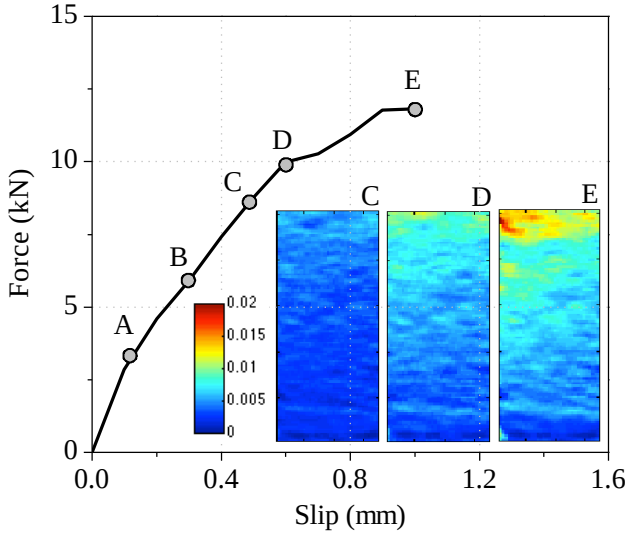

(b)

Fig.12. Strain distribution along the bonded area at different load levels in a typical (a) SF- and (b) RF-specimen.

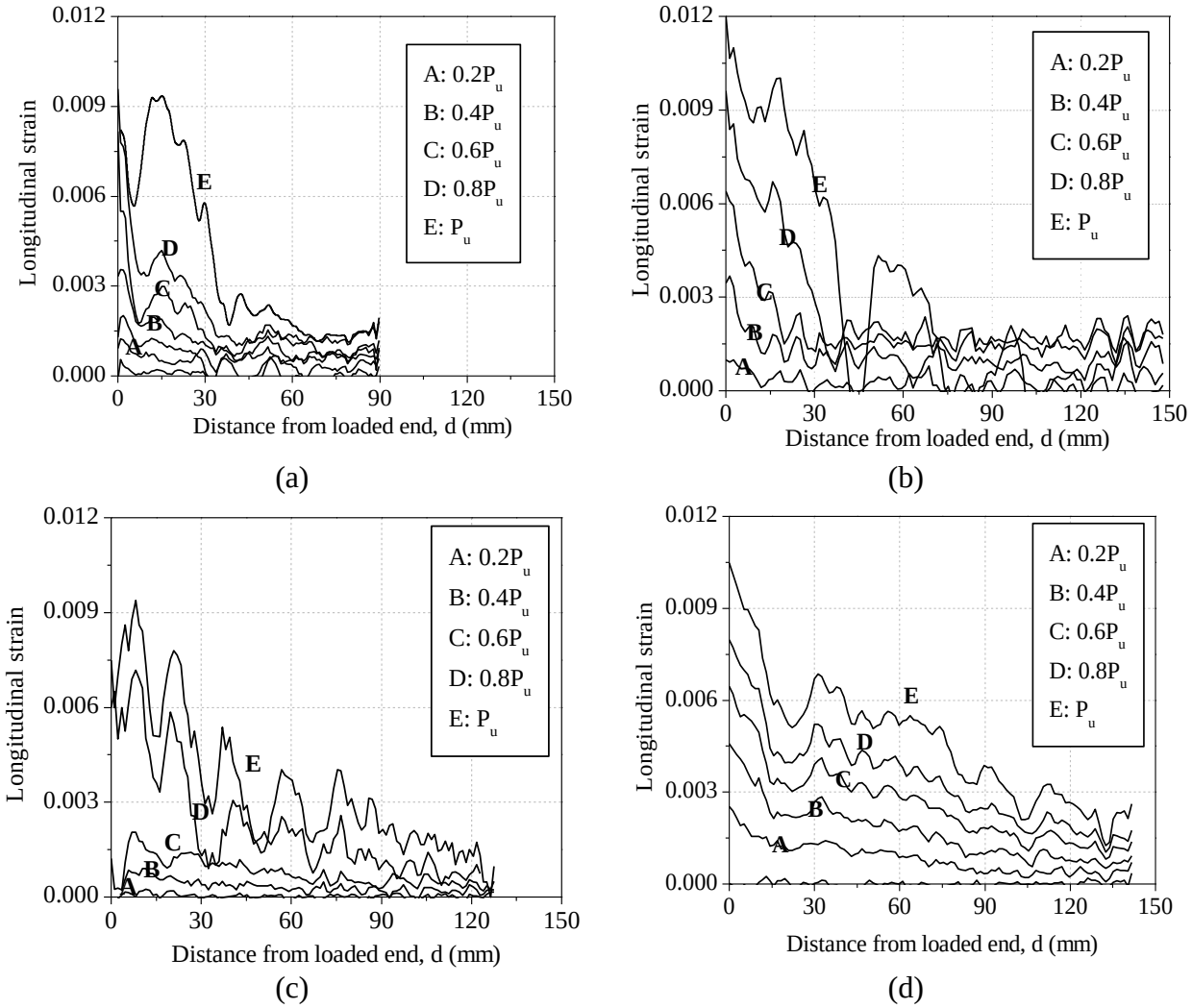

Fig.13. Longitudinal strains distribution in typical (a) SE-; (b) RE-; (c) SF- and (d) RF-specimens. Note that graph (b) has a vertical scale different from the other plots.

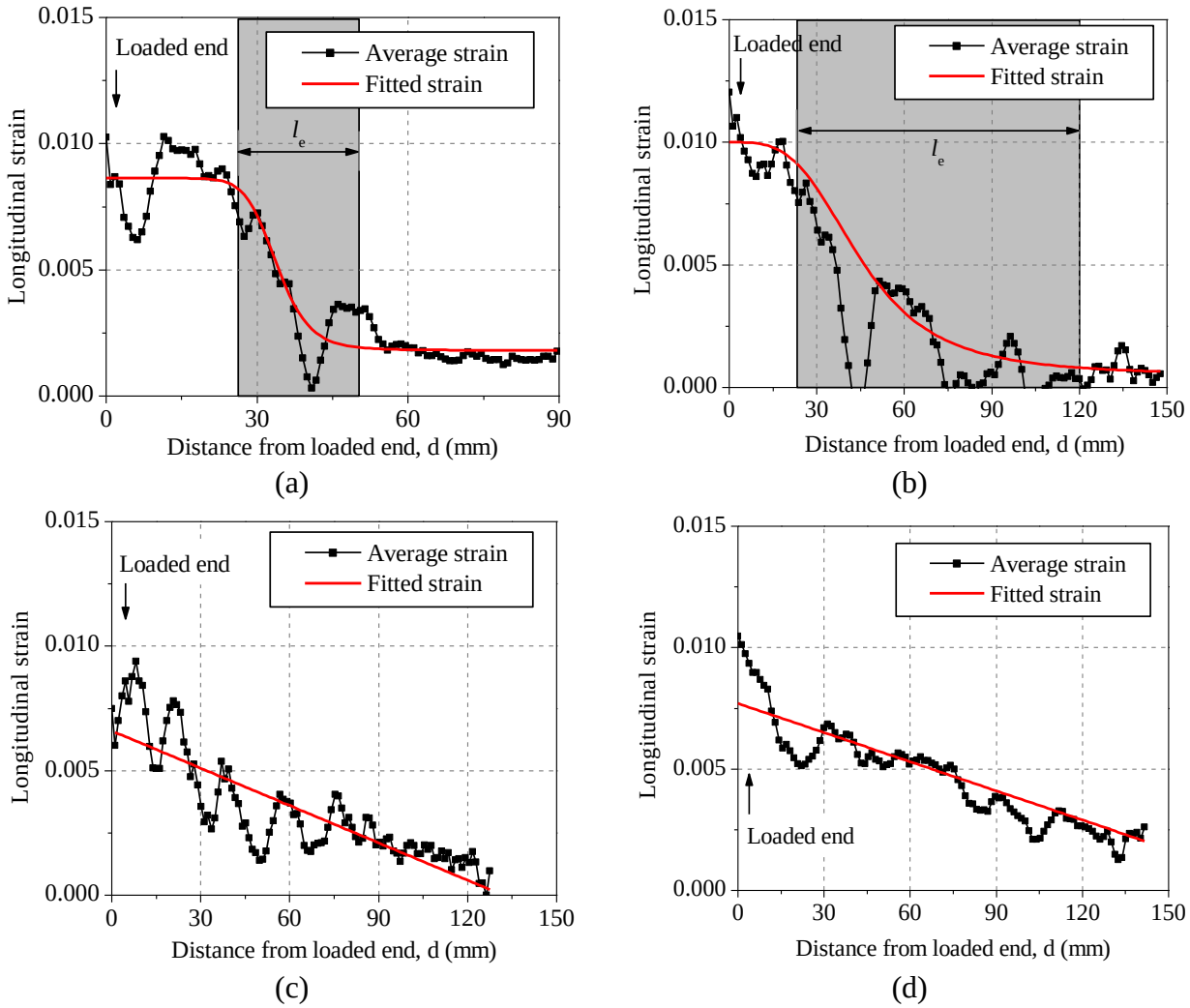

Fig.14. Average longitudinal strain profiles in (at the peak load) (a) SE-; (b) RE-; (c) SF- and (d) RF-specimens.

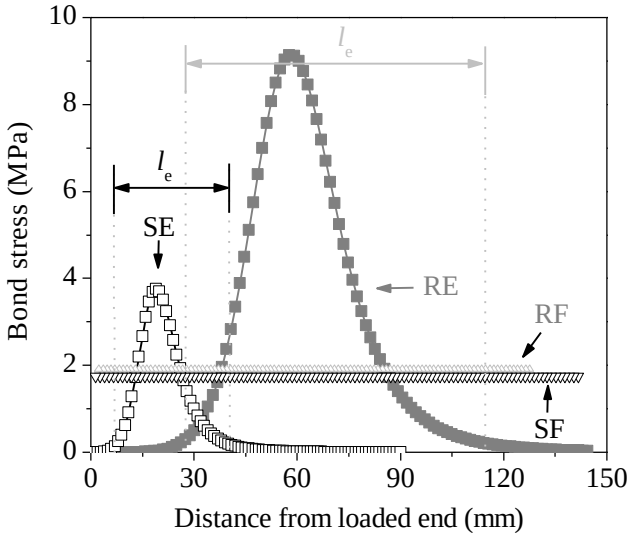

Fig.15. Typical bond stress distribution along the bonded length at the peak load level.

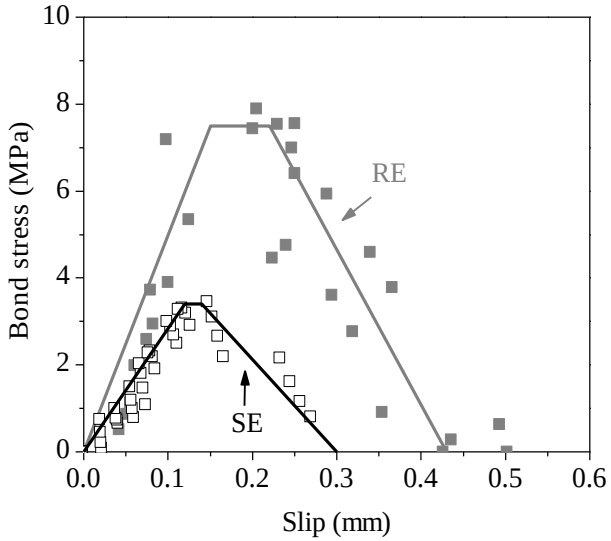

Fig.16. Bond-slip laws obtained for SE- and RE-specimens.

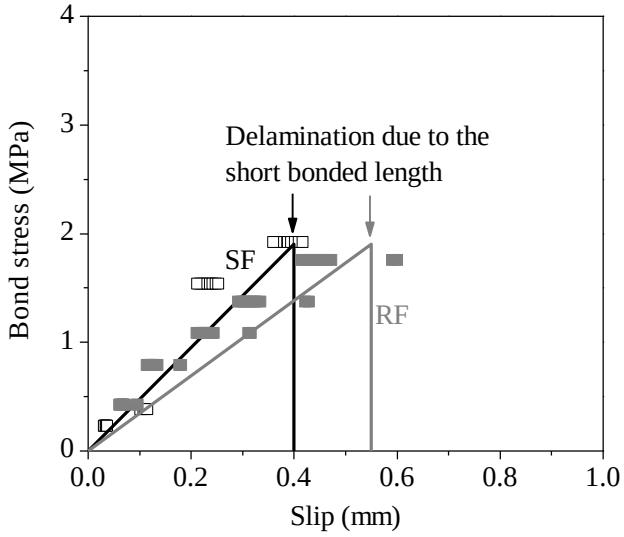

Fig.17. Bond-slip laws obtained for SF- and RF-specimens.